Localized-plasma-assisted rotational transitions in the terahertz region

Yindong Huang,[1,2] Zuoxian Xiang,[2] Xing Xu,[2,3] Jing Zhao,[1] Jinlei Liu,[1] Ruixing Wang,[2] Ziyi Zhang,[2] Zhihui Lü,[1] Dongwen Zhang,[1] Chao Chang,[2,4,*] Jianmin Yuan,[1,5,†] and Zengxiu Zhao[1,‡]

[1]*Department of Physics, National University of Defense Technology, Changsha 410073, Hunan, China*
[2]*Innovation Laboratory of Terahertz Biophysics, National Innovation Institute of Defense Technology, Beijing 100071, China*
[3]*Aerospace Information Research Institute, Chinese Academy of Sciences, Beijing 100094, China*
[4]*Department of Engineering Physics, Tsinghua University, Beijing 100084, China*
[5]*Department of Physics, Graduate School of China Academy of Engineering Physics, Beijing 100193, China*

(Received 3 April 2020; revised 21 September 2020; accepted 25 January 2021; published 15 March 2021)

Molecular spectroscopy is a powerful tool for accelerating advances in materials science, chemistry, biology, and astronomy. Typically, molecular spectroscopy uses nanotips or nanoparticles to locally detect the molecule properties in a sample resulting from absorption of infrared and terahertz radiations. Here, we present an alternative that transient localized plasma can be applied to enhance the molecular spectroscopy. Our experiments show a significant enhancement of rotational transitions in carbon monoxide plasma under the illumination of terahertz waves. We proposed a semiclassical model for this enhancement, dominated by the energy exchange from electrons to molecules or ions via a collision process in the localized plasma. Our findings gain more insight into the nonequilibrium dynamics in laser-generated localized plasma. We also propose that the localized plasma can be used to improve the sensitivity of molecular spectroscopy.

DOI: 10.1103/PhysRevA.103.033109

I. INTRODUCTION

Molecular spectroscopy at the terahertz and microwave scale is widely applied in molecular composition identification [1,2], chemical reaction analysis [3,4], environmental monitoring [5,6], and astrophysics [7,8]. Large-scale mapping of microwave emissions from carbon monoxide (CO) in the molecular clouds of the Milky Way provides detailed information on the pressure, position, components, and formation of remote galaxies [8–10]. These waves can also be applied directly to reveal the activities of hydrogen bonds that are prominent in life science [11]. Nowadays, the continuous progress of terahertz sources and detectors makes it possible to quickly and accurately characterize the fingerprint spectral content of molecules [4,12–17]. The renewed efforts, such as hydrogen bond networks [18], solution dynamics [19,20], two-dimensional Raman spectroscopy [3,21,22], and remote sensing of gas [23], have combined the fields of terahertz and chemical technologies and shed light on the fields of terahertz chemistry and terahertz astronomy.

When using terahertz or infrared waves to detect the spectrum and dynamics of matter, the local-field enhancement is a popular method to improve the sensitivity and the spatial resolution by coupling the light with the nanotips and nanoparticles [24–29]. Besides these nanostructures, plasma can be an alternative. Laser-generated plasma is in a nonequilibrium state that confines a large quantity of hot electrons and ions. Under the external field, these hot electrons are easily polarized and collide with the neighboring particles, producing stimulated emissions [30,31], enhanced fluorescence [32–34], and terahertz echoes [35]. The collective motions of these electrons can work like resonators [36–38] as the electrons in nanotips do, and then realize a local-field enhancement at the boundary and the plasma inside. Moreover, the plasma oscillation frequency of the laser-generated localized plasma coincidentally falls within the terahertz frequency range [37,39]. Therefore, it offers a unique possibility of replacing the nanotips or nanoparticles with the cold plasma for the local-field assisted terahertz detection.

In this work, we took advantage of the localized plasma and performed transient terahertz absorption spectroscopy (TTAS) to study the rotational transition of a CO-formed plasma. Compared with the absorption from pure neutral CO gases, we found that the absorption profile of the formed plasma showed two distinct features: first, a broad resonance absorption background due to the localized plasma, and second, an enhanced rotational absorption by the neutral CO molecules assisted by the plasma. Our semiclassical model reproduced the enhancement feature qualitatively and identified the nonequilibrium dynamics that were based on collisional energy transfer from the terahertz-driven electrons to the polar molecules in the localized plasma.

II. EXPERIMENTAL METHODS

The experimental setup consisted of a titanium sapphire femtosecond laser system and a gas cell for generating plasma, as shown in Fig. 1. The laser system provided 800-nm pulses of 100 fs duration. The laser beam was split into three

*changc@xjtu.edu.cn
†jmyuan@nudt.edu.cn
‡zhaozengxiu@nudt.edu.cn

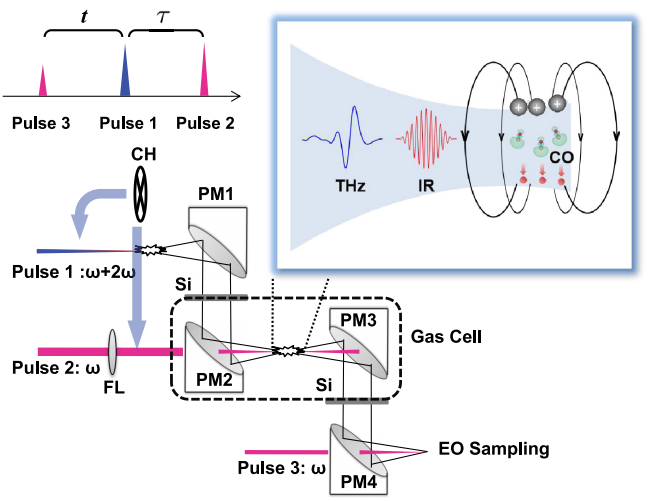

FIG. 1. Schematic of the experimental setup. CH, chopper; Si, silicon window plate; PM1–PM4, parabolic mirrors; FL, focusing lens. The blue arrows indicate the positions in which to place the chopper for different measurements. The top right inset shows the sequential illumination of CO molecules under the infrared laser and the terahertz wave, which generates plasma and drives the electrons to form the modulation fields, respectively.

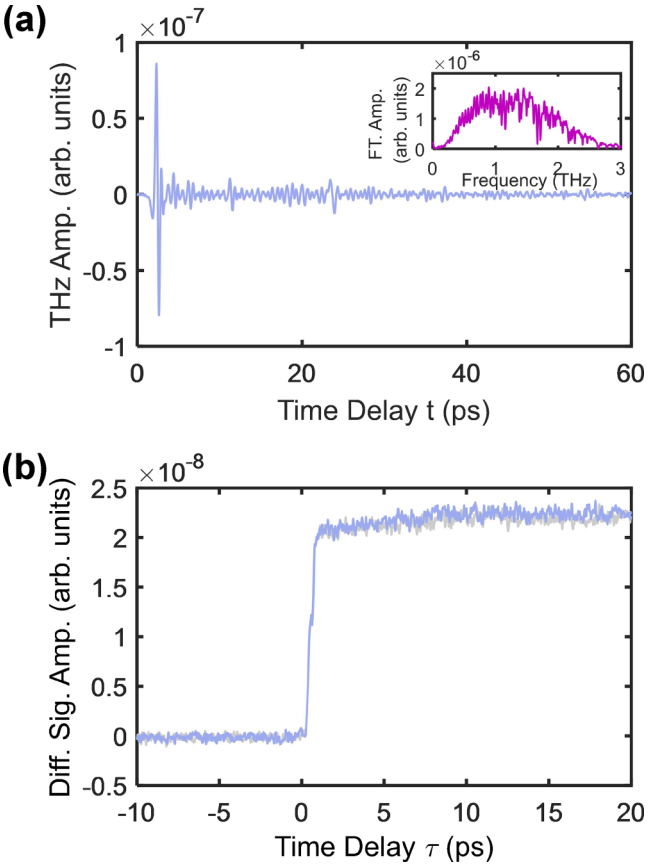

FIG. 2. (a) A typical terahertz time-domain spectrum was measured by placing the chopper on the arm of pulse 1. The inset shows the Fourier-transformed terahertz amplitude. (b) The differential signal (DS) amplitude was measured as a function of the time delay τ between pulse 1 and pulse 2. The DS was obtained by placing the chopper on the arm of pulse 2.

parts: for terahertz wave generation (pulse 1), the formation of plasma (pulse 2), and the electro-optic sampling of the transmitted terahertz waveform (pulse 3). In pulse 1, the terahertz wave was generated by the collinearly propagating dual-color laser fields, whose relative phase could be adjusted to maximize the terahertz output. The intensities of the fundamental pulse and the second harmonic pulse in pulse 1 were estimated to be 2.5×10^{14} and 2.6×10^{13} W/cm^2, respectively. The plasma was prepared by using the focusing laser, pulse 2, to provide the freed electrons. The peak intensity of this pulse was estimated to be 1.7×10^{14} W/cm^2. The chopper could be placed on the arm of pulse 1 or pulse 2 to detect the transmitted terahertz waveform or the differential signals (DSs) [40,41].

The gas cell was used to avoid leakage of toxic CO molecules. Most gas cell areas were vacuumed by a dry pump, allowing a supersonic expansion of the gas molecules from a laser-cut glass capillary. The CO molecules were therefore concentrated mainly around the nozzle of the gas capillary. To ensure that terahertz waves penetrate the entire plasma regions, collinear pulse 2 and terahertz waves were sequentially focused downstream of the nozzle. The scheme is sketched in the top right inset of Fig. 1. The laser output remained unchanged to ensure a stable terahertz radiation during the whole measurement. The backing pressure in the nozzle could be varied to offer different electron densities of the plasma. The amplitude of the transmitted terahertz waveform (or the DS) was traced by a 1-mm-thick (110)-cut electro-optic zinc telluride (ZnTe) crystal. Figure 2(a) shows one typical terahertz time-domain spectrum measured by placing the chopper on the arm of pulse 1. Its peak intensity was calibrated to be 0.9 kV/cm and its dynamic range was about 500:1. The Fourier-transformed terahertz amplitude can be seen in the upper right corner of Fig. 2(a). In Fig. 2(b), we show the DS of the peak amplitude of the terahertz wave, i.e., $t = 2.3$ ps, dependent on the time delay τ between pulse 1 and pulse 2. This helped to pinpoint the moment of temporal overlapping of the terahertz wave and the plasma [37].

To remove the Fabry-Pérot effect caused by the reflection of the chamber windows or the mirrors, we compared the Fourier-transformed terahertz spectra from three cases: one passing through the neutral nitrogen (N_2) gas, one passing through the neutral CO gas (labeled as case I), and the other one passing through CO-formed plasma (labeled as case II). The Fourier-transformed terahertz amplitude of neutral N_2 served as a reference, i.e., $E_{\mathrm{ref}}(\omega)$, because neutral N_2 gas does not exhibit significant absorption on the detecting frequency range. Meanwhile, the rotational constant of a CO molecule is only 1.93 cm^{-1} ($\sim$0.24 meV), far less than the lowest vibration energy ($\sim$0.26 eV); thus, we ignored the vibrational transition in the following analysis.

We used a focusing terahertz light path differently from the typical absorption measurements using a plane terahertz wave [42,43]. To avoid possible deviation of the estimated effective thickness of the interaction volume, we compared the absorbances (i.e., nearly raw spectra) instead of the commonly applied absorption coefficients. CO molecules, diffusing from

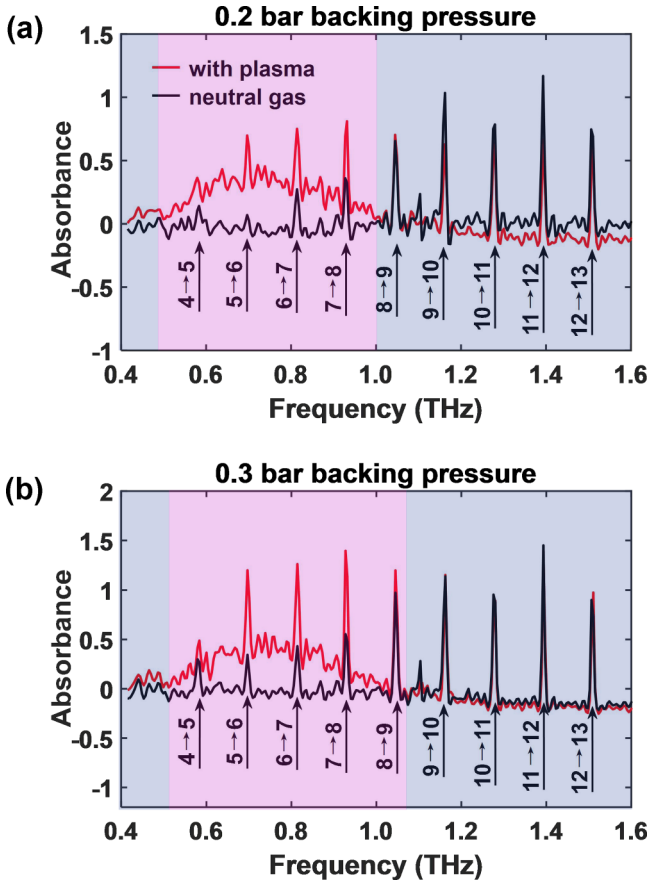

FIG. 3. The absorbance of a terahertz waveform through the CO-formed plasma (red lines) and through the neutral CO gas (black lines) under (a) 0.2 bar and (b) 0.3 bar backpressure. The pink regions indicate the screening dynamics' absorbance of rotational transitions. The black arrows with numbers indicate the rotational transition from state J to state J' $(=J+1)$.

the nozzle to the vacuumed gas cell, were mainly concentrated around the output nozzle; thus, we assumed the same interaction volume for both the neutral CO molecules and the plasma. We followed the method reported in Ref. [39], which treated the plasma volume as a cylinder with uniform electron density N_e. The external terahertz wave was regarded as uniform for the entire plasma volume. More analysis can be found in Appendix B.

III. RESULTS

The obtained absorbances of the terahertz wave $\alpha(\omega) = -\ln\left(\mathrm{I_{CO}}(\omega)/\mathrm{I_{ref}}(\omega)\right)$ are shown in Fig. 3 as two cases of backpressure. The black lines in Fig. 3 indicate the absorbance of the terahertz wave for the neutral CO gas, and the red lines for the CO-formed plasma. Both exhibit sharp absorption peaks, which originate from the transitions between the neighboring rotational states. The difference between them can be ascribed to the plasma effect on the absorption property as highlighted by the pink regions in Fig. 3. Clearly, a broadband resonance absorption is significant in these regions, which lifts the baseline. This resonance absorption was caused by the dynamic spatial separation of electrons and ions within the plasma under the exposure of an external terahertz field [37]. As the backpressure increased, the central frequency of the resonance slightly shifted to a high frequency. Notably, the rotational absorption lines were enhanced in the pink region on top of the broadband resonance absorption.

At 0.2 bar of backpressure, as shown in Fig. 3(a), the enhanced line of rotational absorption centers around 0.69 THz, corresponding to the rotational transition from state 5 to state 6. For the 0.3 bar of backpressure in Fig. 3(b), the enhanced terahertz absorption line centers at 0.80 THz, corresponding to the rotational transition from state 6 to state 7. The shift of the central frequency with pressure is in accordance with that of the plasma absorption, suggesting that there is related physics behind it.

To understand the enhancement of rotational transition, the transition line strengths and line shapes of the spectra were compared between the neutral CO gas and the CO-formed plasmas. We will start with neutral gases. In our experiment, the field strength of the incidental terahertz wave was so weak that we ignored the nonlinear effects. The rotational absorbance of the terahertz wave by neutral molecules at frequency ω can be written as [44]

$$\alpha_{\mathrm{rot}}(\omega) \simeq \sum_{J} N_0 \Delta f(J) L_{JJ'} \mathrm{Im}\left[\frac{\omega}{\Omega_{JJ'}^2 - \omega^2 - i\Gamma\omega}\right], \quad (1)$$

where N_0 is the number of molecules, $\Omega_{JJ'}$ is the frequency of rotational transition between the state J and the state J' $(=J+1)$, and $\Delta f(J)$ is the difference of population between these two rotational states. The linewidth Γ is related to the relaxation time of the coherence $\Gamma \simeq 2\pi/\tau_{\mathrm{coh}}$, which is estimated at about several hundred picoseconds [45]. By fitting our experiment, we found that the linewidth of about 0.01 THz was consistent with previous work. $L_{JJ'}$ is the absorption strength between the two rotational states, which could be expressed as

$$L_{JJ'} = \frac{4\pi\mu_x^2 S_{JJ'}^{(x)} \Omega_{JJ'} \langle\cos^2\theta\rangle}{hc}, \quad (2)$$

where μ_x is the projection of the dipole matrix element on the molecular axis and $S_{JJ'}^{(x)}$ are the quantities to calculate the transition strength [44]. θ is the angle between the molecular axis and the polarization of the laser field, h is the Planck constant, and c is the velocity of light. Note that the term $(\Omega^2 - \omega^2)$ is in the denominator of the last term of Eq. (1), which means that only when the frequency ω of incident terahertz light coincides with the rotational transition frequency $\Omega_{JJ'}$ does the rotational transition absorption become significant.

Next, we looked at the TTAS of CO-formed plasma. Because the density of ions created by the laser in the plasma was much less than that of the neutral molecules (as shown later), we ignored the absorption from the rotational transition of ions. Free electrons in plasmas are driven by the incidental terahertz wave to depart from ions, creating a localized field with an opposite polarization [37,41]. This could be viewed as a combination of the terahertz-electron interaction and the resulting screening effect of the free electrons discussed above. The local field amplitude E_{loc} is obtained by using the external field E minus the polarization P induced by the spatial separation of the free electrons and residual ions, i.e.,

$E_{\rm loc} = E - P_e/2\varepsilon_0$, with ε_0 the vacuum permittivity. Here, the external terahertz field was linearly polarized and parallel with the polarization of electrons in our experiment. The explicit expression of P_e can be directly obtained from the electron current density, $dP_e/dt = -eN_e dx/dt$, with x representing the displacement of electrons. The displacement x of electrons can be solved using the displacement equation [37]. We define the factor ξ to characterize the field modulation

$$\xi = \frac{E_{\rm loc}}{E} = -\frac{\omega^2 + i\gamma\omega}{\omega_p^2/2 - \omega^2 - i\gamma\omega}, \tag{3}$$

where $\omega_p \equiv \sqrt{(N_e e^2)/(\varepsilon_0 m_e)}$ is the plasma frequency and γ is the damping rate.

With the knowledge of rotational transition absorption in Eq. (1) and the field modulation factor in Eq. (3), the total absorbance in plasma can be expressed as a summation of the resonance absorption term and the rotational transition term,

$$\begin{aligned}\alpha'(\omega) &= \alpha_{\rm res} + \alpha'_{\rm rot} \\ &\simeq \frac{\omega}{c}{\rm Im}\left[\frac{\omega_p^2}{\omega_p^2/2 - \omega^2 - i\gamma\omega}\right] \\ &\quad + \sum_J N_0 \Delta f'(J) L_{JJ'} |\xi| {\rm Im}\left[\frac{\omega}{\Omega_{JJ'}^2 - \omega^2 - i\Gamma'\omega}\right],\end{aligned} \tag{4}$$

where the first term is for the broadband resonance absorption of plasma introduced by the screening dynamics of the electrons in the localized plasma, and the second term indicates the rotational absorption in plasma. The parameter Γ' indicates the relaxation of rotation in CO-formed plasma, which can be obtained by fitting the experimental results. In principle, the molecular and electron motions in the terahertz field should be solved jointly, while here we separated them. The collective motion of free electrons was simplified as a field modulation factor, and we used a localized field instead of the electron current in analyzing the molecular rotational transition. It should be noted that the unprimed and primed notations are for pure CO gas and CO in plasma, respectively, except for the rotational quantum number J'.

The resonance absorption of electrons and the rotational transition absorption can be fitted by the two parts of Eq. (4), respectively. To compare the rotational absorbance in Eqs. (1) and (4), we defined an enhancement factor β to calibrate the enhancement of the rotational transitions from state J to J' between the neutral gas and the plasma,

$$\beta \equiv \frac{\alpha'_{\rm rot}(\omega = \Omega_{JJ'})}{\alpha_{\rm rot}(\omega = \Omega_{JJ'})} \simeq |\xi| \frac{\Gamma \Delta f'(J) \langle \cos^2\theta' \rangle}{\Gamma' \Delta f(J) \langle \cos^2\theta \rangle}. \tag{5}$$

Here, the enhancement factor β was a function of the rotational excitation energy and was obtained by taking the ratio of the height of the peak in the line shape for each J.

The rotational distributions could be rearranged because of the interaction between the strong laser field and the laser-induced polarization, known as "molecule alignment" [46]. We calculated the angular momentum redistribution of CO molecules at 100 K rotational temperature to show the alignment's effect on molecular rotational absorption. The calculation method is presented in Appendix G. The blue line with circles in Fig. 4(a) exhibited the initial J-state distribution of the thermal CO molecules, which followed the Boltzmann distribution. The population of the rotational states, excited by the intense femtosecond lasers, is modulated by rotational Raman transitions. The average value of J is shifted to a higher value as we increase the laser intensity. The laser-excited coherent rotational wave packet [red dashed line in Fig. 4(a)] cannot be directly applied in Eq. (5), because this equation works for the thermal molecules. In the classical rotational absorption model, the alignment-correlated term only appears in $\langle \cos^2\theta \rangle$ [Eq. (C8) in Appendix C). Then, we focus on the alignment contribution $\langle \cos^2\theta \rangle$ in Eq. (5). Coherence between rotational states can induce a quantum beating of the alignment contribution $\langle \cos^2\theta \rangle$, whose value exhibits a sudden oscillation every 4.3-ps interval. As shown in Fig. 4(b), the baseline of $\langle \cos^2\theta \rangle$ took about 0.36, which was nearly the same as the value of 1/3 for randomly aligned molecules. The incoherent alignment of molecules caused this minor rise [47]. Typically, the oscillation of the value of $\langle \cos^2\theta \rangle$ lasts for only a few hundred femtoseconds, whose timescale is extremely shorter than the picosecond terahertz waves. Therefore, the

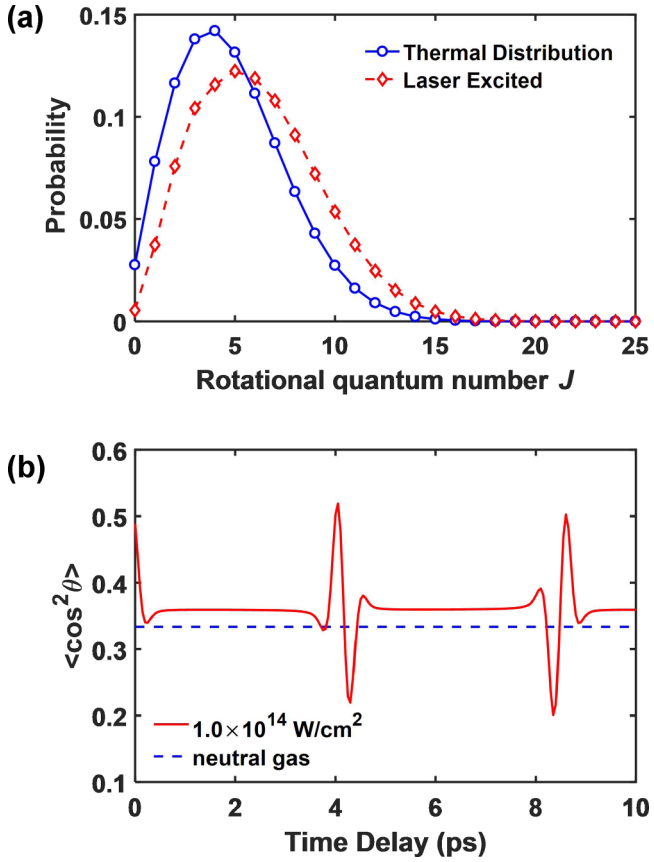

FIG. 4. (a) Calculated redistribution of the rotational states of the CO molecules stimulated by the femtosecond laser. The blue line with circles denotes the Boltzmann distribution of different rotational states J under 100 K rotational temperature. The coherent J-state distribution of the initially unaligned thermal CO molecules is redistributed by rotational Raman transitions that occur in the presence of the laser pulse, whose intensity is 1.0×10^{14} W/cm^2 (dashed red line with diamonds). (b) The calculated $\langle \cos^2\theta \rangle$ for the laser-excited CO ensembles (red solid lines) and the neutral CO molecules (blue dashed lines) are compared.

difference between $\langle\cos^2\theta'\rangle$ and $\langle\cos^2\theta\rangle$ can be neglected in considering the alignment contribution of enhancement factor β, i.e., $\langle\cos^2\theta'\rangle/\langle\cos^2\theta\rangle \simeq 1$.

Furthermore, the transition rate Γ' approximates to Γ because the rotational transition lines between neutral gas and plasma (shown in Fig. 3) are similar in width. By fitting the experimental result, it was found that the full width at half maximum (FWHM) of coherent rotational transition was about 10^{10} Hz, corresponding to the 600-ps decay time for coherent rotations of the CO molecules. This was at the same magnitude as the result of the free induction decay experiment on other small molecules [45]. Finally, we obtained a reduced form of Eq. (5), which is $\beta \simeq |\xi|\Delta' f(J)/\Delta f(J)$. The factor $|\xi|$ implies the origin of enhanced rotational transitions and why they are located within the broadband resonance absorption.

To further clarify the analysis, we used the rotational transition of CO under the 0.3 bar to demonstrate. As shown in Fig. 5(a), the plasma frequency ω_p was estimated to be $2\pi \times 0.85$ THz and the collision rate γ was about 3×10^{12} s^{-1} by fitting the Lorentz-like broadband resonance absorption. It should be noted that, in order to improve the quality of the fitting of the broadband resonance absorption, a small baseline offset is applied here. The electron density N_e can be calibrated as 8.6×10^{15} cm^{-3}. The majority of the ions were assumed to be single charged due to the plasma being prepared by tunnel ionization; thus, we obtained $N_i \simeq N_e$. The concentration of the neutral gas molecules N_0 at the 0.3 bar was estimated to be 8.1×10^{18} cm^{-3}. The enhancement factors β of rotational transition between $J = 4$ and 12 are shown in Fig. 5(c), as well as the calculated $|\xi|$, by using the fitting parameters of plasma. The experimentally deduced β and the calculated $|\xi|$ exhibit a similar trend, indicating that our interpretation, based on the dynamic screening of the electrons in the external terahertz field, was correct, though there is a divergence in the absolute value. This divergence could be attributed to the redistribution of rotational population.

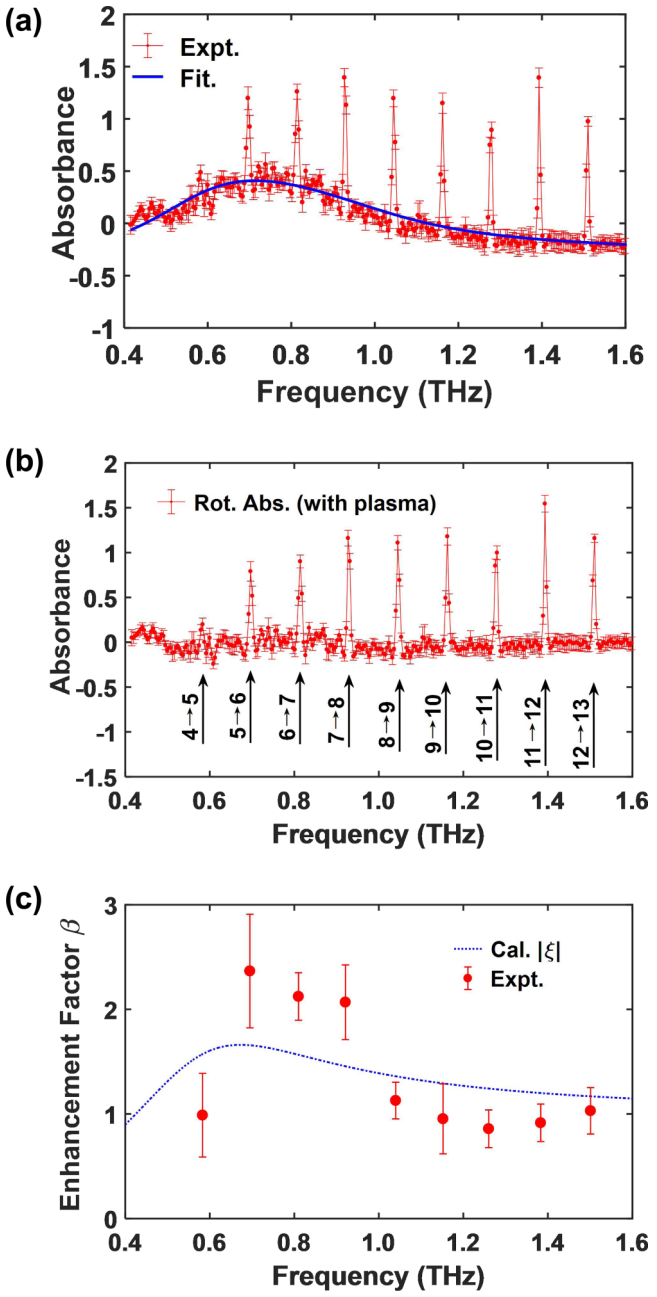

FIG. 5. (a) The experimentally deduced absorbance of CO-formed plasma (red lines) and the fitted resonance absorption (blue lines) appear under the 0.3 bar. A small baseline offset is applied for a better fit. (b) The enhanced rotational absorbance in the plasma, which was obtained by subtracting the two curves in (a). The black arrows show the corresponding rotational transitions. (c) The experimentally deduced enhancement factors β (red solid dots) for different rotational transitions were compared with the calculated values of $|\xi|$ (blue dotted lines).

IV. DISCUSSIONS

We can justify our argument based on energy exchange. A single electron cannot directly absorb or lose energy under an external field, but the energy of an electromagnetic wave can be transferred from electron to molecule or hole because of collision [40,48]. Under the external terahertz wave field, it has been suggested that collision between electrons and molecules enables the enhancement of fluorescence [32], which is the energy transfer between the applied terahertz field and the molecules via a collision process [49], as shown in Fig. 6(a). Here, the rotational redistribution of molecules may come from a similar process. In Fig. 6(b), we compared the differences of rotational population $\Delta f'(J)$ deduced from experiments by using Eq. (5) (red line with circles) and calculated from the coherent rotational wave packet excited by the laser (blue line with squares). However, neither the thermal distribution nor the coherent rotational wave packet is consistent with the experimentally deduced J-states distribution, implying the existence of other dynamics in plasma. The free electrons are driven by the external terahertz field, resulting in field modulation (localized polarization) caused by the separation of the free electrons and the remaining ions. These electrons then collide with the molecules and ions in the plasma. The energy exchange between free electrons and ions introduces broadband resonance absorption [37], indicating that laser-generated plasma is a good energy storage medium in the terahertz band. This might also be the reason

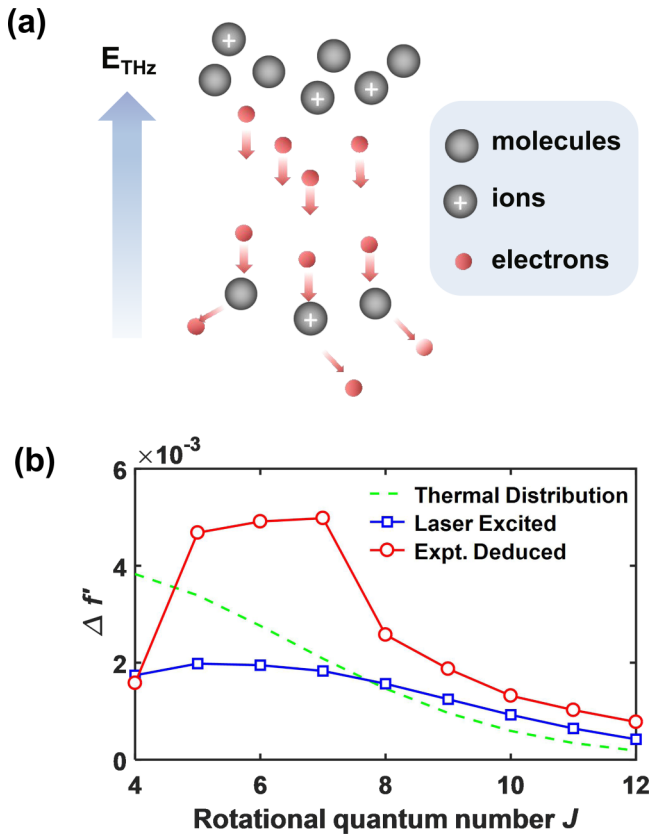

FIG. 6. (a) Electron acceleration in the terahertz field and collision with molecules and ions. The electron-molecule collision induces an enhancement of rotational transition, $e + \mathrm{CO}\,(J) \rightarrow e + \mathrm{CO}\,(J')$. (b) The red circle lines are the $\Delta f(J)$ of CO molecules in plasma deduced from 0.3 bar experimental results. The blue line with squares shows the calculating results of the coherent rotational wave packet excited by a 100-fs laser pulse at an intensity of 1.0×10^{14} W/cm^2. For comparison, we also show the thermal distribution of different rotational states J under 100 K rotational temperature (green dashed line).

for the spatial confinement of terahertz waves when using air plasma to generate and propagate terahertz emission [50]. In short, localized-plasma-assisted rotational transitions could be viewed as an energy exchange between the molecules and the free electrons via collisions, i.e., $e + \mathrm{CO}\,(J) \rightarrow e + \mathrm{CO}\,(J')$ [51]. For a higher backpressure, the general shape of the terahertz absorbance of CO plasma is the same as those shown in Fig. 3, including a significant broadband resonance absorption and an enhancement of rotational transitions. However, the enhancements of the rotational absorptions appeared at a broader frequency range than the resonance absorption area, which calls for more complex interpretation, such as the multibody collisions in dense circumstances.

Furthermore, localized plasma is especially suitable for promoting the plasma-based terahertz detection and generation technology. On the one hand, the collective motion of electrons in plasma can form a localized field that can greatly improve the absorption of terahertz waves. Typically, the spatial scale of air plasma is on the order of about 100 μm. Even though its scale is much larger than the nanometer-level nanotips, it still has certain advantages because the oscillating frequency of laser-generated plasma is at the terahertz band. The focus size can be further reduced by using high-numerical-aperture (NA) focusing of light [52]. With the help of localized-field-assisted plasma, our method can be implanted into plasma-based medical treatment [53], saving the high cost of atomic force microscopy apparatus [54]. It should also be noted that the present article only gives a quite general and preliminary estimation of plasma, as well as the dynamics inside. Before application, more studies are required on the plasma properties, and on how the enhancements vary with parameters such as the gas pressure, pulse separation times, and intensities of the incident laser and terahertz radiation. For instance, the synchronous measurement of the fluorescence of stimulated emissions can help to characterize plasma at the same time [55]. On the other hand, if the population inversion of the rotational states occurs in plasma, i.e., $\Delta' f(J) < 0$, absorption of the terahertz wave could turn into an emission based on Eq. (5). State-of-the-art tunable terahertz output is obtained by the rotational population inversion in dilute polar molecules [56]. If we can take advantage of the electron collisions ($|\xi|$) and realize a rotational population inversion ($\Delta f'(J) < 0$), it might be possible to generate more intense terahertz wave output in high-density environments.

V. CONCLUSION

In conclusion, we observed a significant enhancement of rotational transitions in CO-formed plasma, which was caused by the collisions between terahertz-wave-driven electrons and molecules in localized plasma. A semiclassical model, based on a field modulation of the separation between the free electrons and the remaining ions, is used to explain the experimental results. We showed that the collective motion of electrons colliding with molecules creates an energy exchange between electrons and molecules from the external terahertz wave. Our model disentangles the coupling between the motions of hot electrons and the molecular rotations and provides a comprehensive picture of the nonequilibrium dynamics in plasma. These findings offer unique possibilities for enhancing the electromagnetic field with the assistance of laser-generated plasma instead of the conventionally used nanotips or nanostructures [57]. Other fields of study, such as air breakdown coherent detection [58,59], that utilize optically induced plasmas can benefit from our results. The enhancement of rotational transition also provides an unusual opportunity to develop an intense frequency-tunable narrow-linewidth terahertz laser.

ACKNOWLEDGMENTS

This research was funded by the National Natural Science Foundation of China (Grants No. 11804388, No. 51677145, No. 61905286, No. 11874066, No. 51807203, and No. 11904400), the Major Research plan of the National Natural Science Foundation of China (Grant No. 91850201), and the China National Key R&D Program (Grant No. 2019YFA0307703).

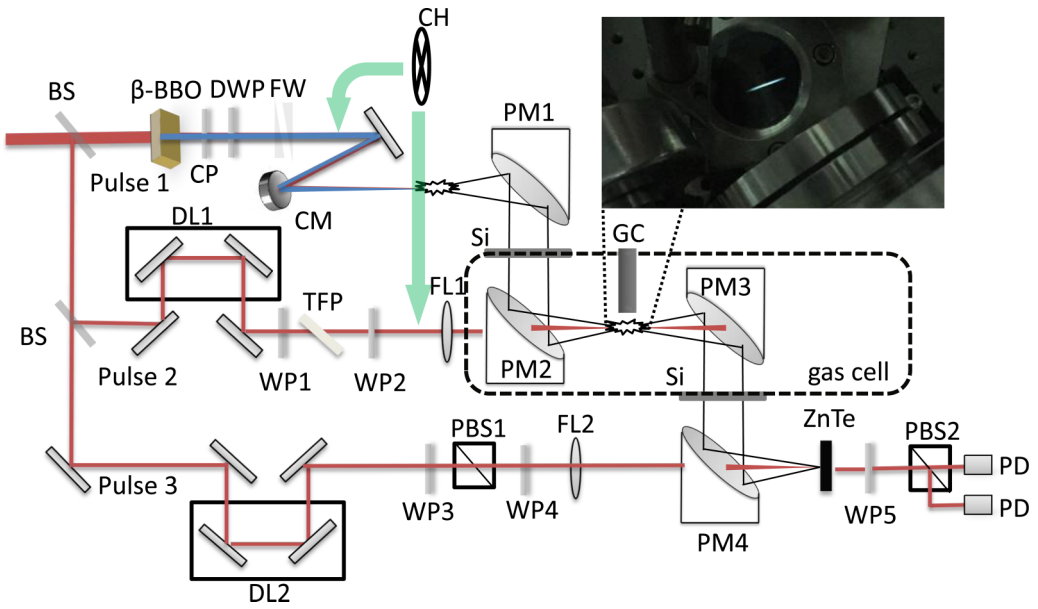

FIG. 7. Experimental setup. BS, beam splitter; CP, compensation plate; DWP, dual-wavelength wave plate; FW, fused silica wedge; WP1–WP4, $\frac{1}{2}\lambda$ wave plate; TFP, thin-film polarizer; CM, concave mirror; DL1 and DL2, delay lines; FL1 and FL2, focusing lenses; GC, glass capillary; PM1–PM4, parabolic mirrors; PBS1 and PBS2, polarizer beam splitters; WP5, $\frac{1}{4}\lambda$ wave plate; PD, photodiode detector; CH, chopper. The top right inset shows the bright fluorescence in CO-formed plasma in the laboratory.

APPENDIX A: DETAILS OF THE EXPERIMENTAL SETUP

The experimental setup is shown in Fig. 7, which consists of a 1-kHz, 4.4-mJ, 100-fs Ti:sapphire amplifier with central wavelength of 800 nm and the gas cell for generating CO plasma. The output laser beam was split into three parts: for terahertz wave generation (pulse 1), the formation of plasma (pulse 2), and the electro-optic sampling of the transmitted terahertz waveform (pulse 3).

The generation pulse (pulse 1) passes through a 100-μm-thick type-I beta barium borate (β-BBO) crystal to produce the second harmonic of the fundamental field. A 5-mm-thick α-BBO provides a negative dispersion to the two-color fields, which is served as a compensation plate for the group velocity dispersion introduced by the wedges and dual-wavelength plate. The polarizations of the two-color fields are rotated to be parallel by a dual-wavelength wave plate, which is a full-wave plate for the 400-nm pulse and a half-wave plate for the 800-nm pulse. A pair of fused silica wedges is placed to achieve the maximum output of the terahertz wave by precisely controlling the relative phase between the two colors. Delay line 1 (DL1) is used to control the time delay τ between pulse 1 and pulse 2. It should be mentioned that the laser intensities might be overestimated, because we do not consider the intensity clamping within the filament in estimating the intensities. A hole-drilled off-axis parabolic mirror (PM2) reflects the terahertz wave generation and leaks the plasma-prepared pulse 2 jointly. Pulse 3 is used to track the terahertz waveform by a 1-mm-thick (110)-cut zinc telluride (ZnTe) crystal. Delay line 2 (DL2) is used to vary the time delay t between Pulse 2 and Pulse 3. The output signals from the balanced detectors (PDs) record the terahertz waveform when placing the chopper at the arm of pulse 1, or record the differential signal (DS) by placing the chopper at the arm of pulse 2. The details of the arrangement of the chopper, as well as the analysis of the output signal, can be found in Ref. [37].

APPENDIX B: ANALYSIS OF THE EFFECTIVE THICKNESS OF THE INTERACTION VOLUME

In the experiment, most gas cell areas remained in vacuum, so the absorption of terahertz waves occurred mainly near the downstream of the nozzle. When pulse 2 was blocked, terahertz waves were absorbed primarily by the neutral CO molecules around the nozzle.

However, when pulse 2 was turned on, gas molecules in the interaction volume were ionized to plasma. Plasma filament was generated through an extremely nonlinear process of the focusing laser pulses. According to the tunneling-ionization model [60,61], the ionization probability is exponentially dependent on the field strength. In other words, the electron density in plasma relies on the spatial intensity distribution of the incident laser pulse. Before focusing on the gas cell, the transversal intensity of pulse 2 obeyed a two-dimensional Gaussian distribution; thus, the focusing pulse was symmetrical to the central axis of the filament. However, since the laser field is clamped down to a maximum value due to the intensity clamping effect in plasma [62,63], we assumed that the electron density therein only experiences a little change in the transverse. It means that plasma filament can be treated as a relatively simple geometry that was a cylinder with a uniform electron density [39], as shown in Fig. 8(a). This treatment allows us to determine plasma properties for the experiment. For instance, the free electron density of plasma can be deduced from the central frequency of the resonance absorption, and the frequency range of the broadband resonance absorption associates with the momentum scattering time of these electrons.

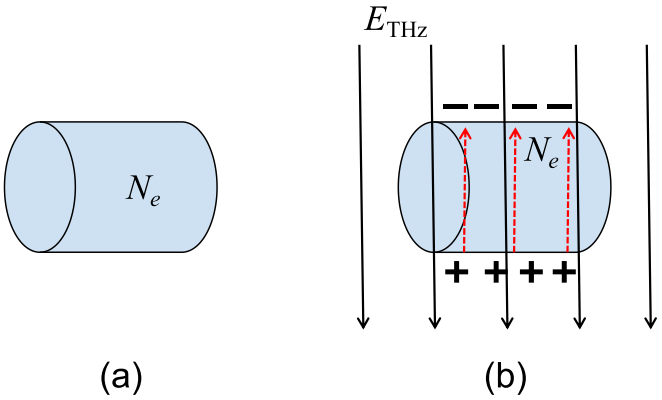

FIG. 8. (a) The filament is regarded as a cylinder with uniform electron density N_e. (b) The terahertz field is considered as a uniform electric field for the cylinder shape filament. The black solid lines indicate the effective uniform terahertz fields with the field strength E_{THz}, while the red dashed lines sketch the screening field formed by the spatial separation between the electrons and the remaining ions.

Since the transverse diameter of plasma was much smaller than the terahertz beam in the waist, we ignored the terahertz strength's spatial characteristics in the plasma volume and regarded the terahertz field as a uniform electric field. The scheme is sketched in Fig. 8(b). We used the least-squares method to evaluate plasma frequency, momentum scattering time, and the plasma filament's effective thickness. The effective thickness of the filament is about 320 microns. The effective electron density can also be obtained from $\omega_p = \sqrt{(N_e e^2)/(\varepsilon_0 m_e)}$, with ω_p the fitted plasma frequency [37]. In Ref. [39], the filament volume's effective thickness was about 180 microns both from a simple geometrical analysis and from a fitting of experimental results. Their plasma thickness results are on the same order of magnitude as ours, while our result is longer. This is because the plasma-generating pulse and the terahertz wave propagate with a crossing angle in their experiment but collinearly in the present experiment. Interestingly, the fluorescence length of the filament was about 2 cm. It is worth noting that our experiment was carried out at early times after photoionization. The fluorescence length was much longer than the experimentally deduced plasma thickness, showing evidence of plasma expansion in the following processes.

APPENDIX C: ABSORPTION OF TERAHERTZ WAVE IN NEUTRAL GASEOUS CO

We start with a classic model of molecular rotation. Assume that the CO molecule is rigid during rotation; that is, the nuclear distance between the two atoms remains unchanged. The internuclear distances between the C nucleus and the O nucleus and the reduced mass of the CO molecule are denoted as R and μ. The coordinates are established as shown in Fig. 9, where the molecular rotation plane under no external field force is defined as the xy plane. The direction of angular momentum is defined as the z axis. The angle between the electric field E and the z-axis direction is θ, while the azimuth and polar angles of the molecular axis are ϑ and φ, respectively.

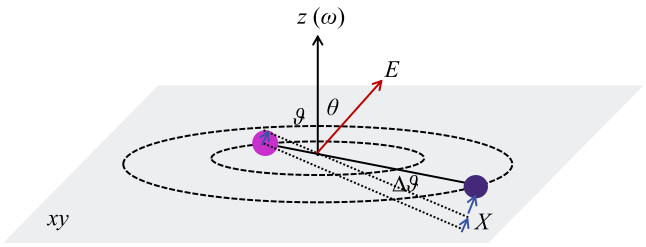

FIG. 9. Coordinates of our formulation.

Under the external field, the Lagrangian of the rotational molecule can be written as,

$$\mathfrak{L} = \tfrac{1}{2} I[\dot{\vartheta}^2 + \sin^2\vartheta\dot{\varphi}^2] - EqR(\sin\vartheta\cos\varphi\cos\theta + \cos\vartheta\sin\theta). \tag{C1}$$

The Lagrangian should be satisfied with the Lagrange equations,

$$\frac{d}{dt}\left(\frac{\partial\mathfrak{L}}{\partial\dot{\vartheta}}\right) - \frac{\partial\mathfrak{L}}{\partial\vartheta} = 0, \quad \frac{d}{dt}\left(\frac{\partial\mathfrak{L}}{\partial\dot{\varphi}}\right) - \frac{\partial\mathfrak{L}}{\partial\varphi} = 0. \tag{C2}$$

When the external field E equals zero, the molecule is free to rotate and the rotational angular momentum is conserved. The steady solutions of Eqs. (C2), noted as Θ and Φ, satisfy

$$\Theta = \pi/2, \quad I\dot{\Phi} = L. \tag{C3}$$

Then, we assume the external field introduces a perturbation to the field-free rotation, thus $\vartheta = \Theta + \Delta\vartheta$ and $\varphi = \Phi + \Delta\varphi$. It means that $\sin\Delta\vartheta \simeq \Delta\vartheta$, $\cos\Delta\vartheta \simeq 1$. Meanwhile, we ignore the higher-order terms of $\Delta\vartheta$ and can obtain the classic motion of a polar molecule under the external field. The equation of $\Delta\vartheta$ can therefore be written as

$$I\frac{d^2\Delta\vartheta}{dt^2} + \frac{L^2}{I}\Delta\vartheta = qRE\cos\theta. \tag{C4}$$

Then, we introduce a variable X, which is the projection of the nuclear distance along the z axis, i.e., $X = R\Delta\vartheta$. We also define the frequency $\Omega = L/I$ and add the damping term $\Gamma\dot{X}$ into Eq. (C4),

$$\ddot{X} + \Gamma\dot{X} + \Omega^2 X = \frac{qE\cos\theta}{\mu}. \tag{C5}$$

The solution of the displacement X can be expressed as

$$X = \frac{qE\cos\theta}{\mu(\Omega^2 - \omega^2 - i\Gamma\omega)}. \tag{C6}$$

The polarization introduced by the rotation of numerous polar molecules under the action of the external field is

$$P_{\mathrm{mol}} = N_0\langle p\rangle = N_0\langle qX\cos\theta\rangle = \frac{N_0 q^2 E\langle\cos^2\theta\rangle}{\mu(\Omega^2 - \omega^2 - i\Gamma\omega)}. \tag{C7}$$

The complex relative dielectric constant caused by the molecular rotational absorption can be written as

$$\varepsilon_m(\omega) = \varepsilon_1 + i\varepsilon_2 = 1 + \frac{N_0 q^2\langle\cos^2\theta\rangle}{\mu}\left(\frac{1}{\Omega^2 - \omega^2 - i\Gamma\omega}\right), \tag{C8}$$

where ε_1 and ε_2 are the real and the imaginary parts of the relative dielectric constant, respectively. Based on Eq. (C8), it exhibits a typical Lorentz line shape of the relative dielectric constant, where $\langle\cos^2\theta\rangle$ indicates the transient alignment of molecules. Coherence of the laser-excited rotational wave packet can last for several tens to hundreds of picoseconds, while the alignment of the rotational wave packet, which is typically characterized by $\langle\cos^2\theta\rangle$ [shown in Fig. 4(b)], experiences a sudden oscillation (hundreds of femtoseconds) every 4.3-ps interval. Therefore, the alignment contribution to the rotational absorption is negligible for the picosecond-scaled terahertz waves.

To give a quantum description of absorption, we can follow the methods in Ref. [64], by replacing q^2/μ by $8\pi^2\nu_{ij}|\mu_{ij}|^2/h$ and replacing Ω by $2\pi\nu_{ij}$. Here $\nu_{ij} = (W_i - W_j)/h$ is the characteristic frequency associated with the rotational transition between the states i and j. Assuming the refractive index n caused by molecular polarization satisfies $n^2 - 1 \ll 1$, and the rotation absorption parameter $\alpha = 2\kappa\omega/c \simeq \varepsilon_2\omega/c$, the rotational absorption can be roughly written as

$$\alpha(\omega) \simeq [N_0]\left[\frac{8\pi^2\nu_{ij}\langle\cos^2\theta\rangle|\mu_{ij}|^2}{hc}\right] \times \left[\mathrm{Im}\left(\frac{\omega}{\Omega^2-\omega^2-i\Gamma\omega}\right)\right]. \tag{C9}$$

In Eq. (C9), the first term is the number of molecular particles that rotate and absorb, the second term corresponds to the intensity of the absorption line, and the third term corresponds to the rotational absorption line shape.

First, we analyze the second term in Eq. (C9), which corresponds to the intensity of the absorption line. Here, μ_{ij} is the dipole moment for the rotational transition from state i to state j, and the probability of different rotational states should be taken into account. Generally, the intensity term can be expressed as

$$\frac{8\pi^2\nu_{ij}\langle\cos^2\theta\rangle[(2J+1)|\mu_{JJ'}|^2 f(J) - (2J'+1)|\mu_{J'J}|^2 f(J')]}{hc\Sigma_j(2j+1)f(j)},$$

with $(2j+1)$ and $f(j)$ the degree of degeneracy and the population of the rotational state j (for $j = J$ or J'). The probability at the rotational state j is the product of the degree of degeneracy and the population, i.e., $(2j+1)f(j)$. Typically, the probabilities of the rotational states follow the Boltzmann distribution, which takes the form of $P_j = (2j+1)e^{-Ej/k\mathrm{T_{rot}}}$, with $\mathrm{T_{rot}}$ the rotational temperature. In Ref. [44], the dipole moment of rotational transition can be expressed as $(2J+1)|\mu_{JJ'}|^2 = (2J'+1)|\mu_{J'J}|^2 = \mu_x^2 S_{JJ'}^{(x)}$, where μ_x is the projection of the dipole matrix element on the molecular axis and $S_{JJ'}^{(x)}$ are the tabulated quantities to calculate the transition strength. Then, we come to a reduced form of Eq. (C9),

$$\alpha_{\mathrm{rot}}(\omega) = [N_0]\left[\frac{8\pi^2\nu_{ij}\langle\cos^2\theta\rangle\mu_x^2 S_{JJ'}^{(x)}\Delta f(J)}{hc}\right] \times \left[\mathrm{Im}\left(\frac{\omega}{\Omega^2-\omega^2-i\Gamma\omega}\right)\right], \tag{C10}$$

where $\Delta f(J)$ is the difference of the rotational population between the rotational state J and state J' $(=J+1)$. Equation (C10) is the same to Eq. (1) in the main text.

APPENDIX D: ABSORPTION OF THE TERAHERTZ WAVE IN CO-FORMED PLASMAS

The resonance absorption caused by the collision between electrons and ions or molecules can be described by the Lorentz-like Drude model [37]. Actually, the plasma frequency is close to the terahertz field frequency, resulting in the broadband resonance absorption. Free electrons cannot absorb energy in the action of the external terahertz field; however, through the collision with molecule and ion particles, the energy exchange can be realized, which is the reason for the broadband absorption of the terahertz wave.

First, we recall the theory of the broadband resonance absorption in the plasma. The displacement x of an electron in plasma can be described by the Drude model [39],

$$m_e\frac{d^2x}{dt^2} + m_e\gamma\frac{dx}{dt} = -eE_{\mathrm{loc}}, \tag{D1}$$

where m_e is the mass of an electron, γ is the damping rate, and e is the electronic charge of the electron. We assume the motion of electrons is faster than that of molecules; therefore, free electrons in plasmas are driven by the incidental terahertz wave to separate from ions, creating a localized field with an opposite polarization [37,41]. The local-field amplitude E_{loc} can be obtained by using the external field E minus the polarization P induced by the spatial separation of the free electrons and residual ions, i.e., $E_{\mathrm{loc}} = E - P_e/2\varepsilon_0$. $P_e = -N_e ex$ is the space-charge polarization due to the charge carriers separating in the field. Here, the external terahertz field was linearly polarized and parallel with the polarization of electrons in our experiment. Due to the effect of the external field, the Lorentz-like line shape appears. That is, the polarization caused by the motion of the electrons can be written as

$$P_e = N_e p = -N_e ex = \frac{\varepsilon_0 E\omega_p^2}{\omega_p^2/2 - \omega^2 - i\gamma\omega}, \tag{D2}$$

where $\omega_p \equiv \sqrt{(N_e e^2)/(\varepsilon_0 m_e)}$ is the plasma frequency. The complex refractive index introduced by the motion of electrons can be expressed as $\varepsilon_e = (\varepsilon_0 E + P_e)/\varepsilon_0 E$.

Therefore, the localized field can be directly obtained from the displacements of electrons, which is

$$E_{\mathrm{loc}} = \xi E = \left|1 - \frac{\omega^2 + i\gamma\omega}{\omega_p^2/2 - \omega^2 - i\gamma\omega}\right| E, \tag{D3}$$

where ξ is the field-modulation factor. By considering the localized field of electrons in plasma, the field strength E from Eqs. (C4)–(C7) should be replaced by the modulated field ξE, with ξ the modulation factor. This also modifies the complex relative dielectric constant in Eq. (C9). Notably, the unprimed and primed notations are for pure CO gas and CO in plasma, respectively, except for the rotational quantum number J'. Now, the rotational absorbance in plasma could be written as a summation of the broadband resonance absorption

and the molecular rotational transition, which is

$$\begin{aligned}\alpha'(\omega) &\simeq \mathrm{Im}\left(\frac{\varepsilon_0 E + P_e + P'_{mol}}{\varepsilon_0 E}\right)\frac{\omega}{c}\\ &= \mathrm{Im}\left[\frac{(\varepsilon_e + \varepsilon'_m)\omega}{c}\right]\\ &\simeq \frac{\omega}{c}\mathrm{Im}\left[\frac{\omega_p^2}{\omega_p^2/2 - \omega^2 - i\gamma\omega}\right]\\ &\quad + \sum_J N_0 \Delta f'(J) L_{JJ'} |\xi| \mathrm{Im}\left[\frac{\omega}{\Omega_{JJ'}^2 - \omega^2 - i\Gamma'\omega}\right],\end{aligned} \tag{D4}$$

where $L_{JJ'}$ is the absorption strength between the two rotational states, which takes the form of $L_{JJ'} = 4\pi\mu_x^2 S_{JJ'}^{(x)} \Omega_{JJ'} \langle\cos^2\theta\rangle/hc$.

APPENDIX E: RELAXATION OF ELECTRONIC DYNAMICS

The collision rate γ in Eq. (D3) includes the collisions between electrons (*e*-*e*), electron-neutral particles (*e*-*m*), and electron-ion particles (*e*-*i*). For this paper, we consider only binary collisions for simplicity. Typically, *e*-*e* collisions conserve the total electron momentum and do not relax the electron current [65]; therefore, we ignore the contribution of *e*-*e* collisions to γ. In Ref. [39], the authors attributed the rate of resonance absorption to the collision between molecules and electrons because of the large concentration difference between the ions and molecules. Nevertheless, other observations suggest that not only the collision between electrons and neutral molecules but also that between electrons and ions should be considered when interpreting the physical meaning of collision rates γ [66].

If an *e*-*m* collision dominates the resonance absorption, the corresponding frequency range should increase significantly with increasing air pressure. However, it can be seen from Fig. 2 in the main text that the FWHM of the absorbance for the 0.2 bar and 0.3 bar were nearly the same. This means that the collision rate does not increase linearly with increasing air pressure. Thus, the possible collision process here should be attributed to the collision between electrons and ions, which means $\gamma \simeq \sigma_{ei} N_i \bar{v}_e$.

The momentum-transfer cross section σ_{en} between a neutral CO molecule and an electron is about 10^{-20} m^2 [67], while the cross section between an ion and an electron, σ_{ei}, is typically 10^6 larger than σ_{en} [48], which means $\sigma_{ei} \sim 10^{-14}$ m^2. N_i is the concentration of the CO ion, which is assumed to be equal to N_e, and $\bar{v}_e$ is the thermal electron velocity. For 0.3 bar backing pressure, the average electronic velocity is of the order of $\bar{v}_e \sim 10^6$ m/s. The effective electron temperature can be roughly estimated to be $T_e \approx 20\,000$ K by using $\frac{1}{2}m\bar{v}_e^2 \simeq \frac{3}{2}k_B T_e$, with k_B the Boltzmann constant. Note that momentum-transfer cross sections σ_{ei} and σ_{en} are functions of the electronic kinetic energy, and thus the distribution function of the electron velocity should be considered if revealing the rigorous plasma temperature [66].

APPENDIX F: RELAXATION OF MOLECULAR ROTATION

In the dilute gas, the main relaxation of molecular rotation comes from the dipole-dipole induced rotation relaxation, whose typical timescale is about a few nanoseconds [56]. Thus, the linewidth of the absorption spectrum corresponding to this kind of relaxation is on the order of gigahertz. Assuming the temperature is 300 K, the rotational relaxation cross section σ_{DD} is about 1.5×10^{-15} cm^2 [68] and the average velocity $\bar{v}_M$ is estimated to be 470 m/s. Therefore, the dipole-dipole collision rate of a CO molecule can be calibrated as $\Gamma_{DD} = N_0 \bar{v}_M \sigma_{DD} \sim 10^8$ s^{-1}. If the molecular rotation temperature increases, the dipole-dipole collision cross section will also increase, but only by a few times, and the corresponding rotational absorption linewidth is still on the order of 10^8–10^9 Hz. However, in our experiments, the FWHM of the rotational transition is about 10^{10} Hz, corresponding to about 600 ps relaxation time of rotation. This is at the same magnitude of the result from the free-induction decay (FID) experiment [45]. In the FID experiment, molecular rotation is coherently excited by a terahertz wave, whose coherent relaxation delay τ is about several hundreds of picoseconds. Similar to the superradiation process [69], the coherent rotational transition may be much faster than the noncoherent case, which here the relaxation is indeed a relaxation of the coherent rotational wave packet excited by the terahertz wave.

APPENDIX G: CALCULATION OF THE LASER-INDUCED ROTATIONAL WAVE PACKET

A femtosecond pulse cannot only generate plasma, but it can also excite the rotational transitions of molecules [70]. This can make a redistribution of rotational states, which is essential to the absorption and emission properties of molecules. In Sec. III, we discuss the effect of molecule alignment introduced by the intense femtosecond laser. Here, we presented the calculation method, which was raised by Ortigoso *et al.* [71].

Assuming that gas molecules have the same state parameters in the region where the molecules interact with the laser, the collective behavior of a large number of molecules can be described by the rotational evolution of a single molecular wave packet. Assuming the molecular rotation wave function is $\Psi(\theta, \phi, t)$, the interaction between the laser field and the molecule satisfies the Schrödinger equation

$$i\frac{\partial\Psi(\theta,\phi,t)}{\partial t} = [B\hat{J}^2 + U(\theta,t)]\Psi(\theta,\phi,t), \tag{G1}$$

where $B\hat{J}^2 = B_0 J(J+1) - D_e J^2(J+1)^2$ is the rotational energy, B_0 is the rotational constant of the CO molecule (with $B_0 = 1.93$ cm^{-1}), and $D_e = 2.79 \times 10^{-10}$ a.u. is the centrifugal distortion coefficient for CO [72]. $U(\theta, t)$ is the potential induced by the electric field on the anisotropic polarizability [71]. The molecular rotational wave function $\Psi(\theta, \phi, t)$ is expanded by the eigenfunction of the rotational motion $|J, M\rangle$,

$$\Psi(\theta,\phi,t) = \sum_J c_J(t)|J,M\rangle, \tag{G2}$$

where c_J is a time-dependent expansion parameters.

Multiplying Eq. (G1) with $\langle\Psi|$ and making an integral, the Schrödinger equation can be expressed as the equations of the expansion coefficients:

$$i\frac{\hbar}{B_0}\frac{\partial c_J(t)}{\partial t} = c_J(t)(\langle J,M|\hat{J}^2|J',M'\rangle - \omega_\perp(t)) - \sum_{J'} c_{J'}(t)\Delta\omega(t)\langle J,M|\cos^2\theta|J',M'\rangle, \quad \text{(G3)}$$

where $\omega_{||,\perp}(t) = \alpha_{||,\perp}E^2(t)/(2B_0)$ and $\Delta\omega = \omega_{||} - \omega_\perp$; $\alpha_{||,\perp}$ is the polarizability of the molecule parallel and perpendicular to the molecular axis. For the dipole transition $\langle J,M|\cos^2\theta|J',M'\rangle$, the selection rule determines that the nonzero crossing terms should satisfy $J' = J, J\pm 2, M' = M$, so Eq. (G3) can be further reduced into

$$i\frac{\hbar}{B_0}\frac{\partial c_J(t)}{\partial t} = c_J(t)[J(J+1) - \omega_\perp(t)] - c_{J-2}(t)\Delta\omega(t)\langle J,M|\cos^2\theta|J-2,M\rangle - c_J(t)\Delta\omega(t)\langle J,M|\cos^2\theta|J,M\rangle - c_{J+2}(t)\Delta\omega(t)\langle J,M|\cos^2\theta|J+2,M\rangle. \quad \text{(G4)}$$

Then, the coefficients $c_J(t)$ of different J can be obtained by solving Eq. (G4). The initial distribution of the rotational states follows the Boltzmann distribution law

$$c_J(t_0) = g(2J+1)\exp\left[\frac{E_J}{k_B T_{\rm rot}}\right], \quad \text{(G5)}$$

where $T_{\rm rot}$ is the rotation temperature of the molecule; g is the weighting factor, which is determined by whether the rotation angle quantum number J is odd or even, and its physical origin comes from the nuclear spin in the molecule. Substituting $c_J(t_0)$ as the initial values into Eq. (G4), and letting it evolve under the laser field, then we can obtain the expansion parameters at the ending time t' of the laser field. These calculated parameters show the redistribution of different rotational states.

[1] G. Scoles, D. Bassi, U. Buck, and D. Lainé, *Atomic and Molecular Beam Methods* (Oxford University Press, New York, 1988), Vol. 1.

[2] C. W. Chou, A. L. Collopy, C. Kurz, Y. Lin, M. E. Harding, P. Plessow, T. Fortier, S. Diddams, D. Leibfried, and D. R. Leibrandt, Science **367**, 1458 (2020).

[3] I. A. Finneran, R. Welsch, M. A. Allodi, T. F. Miller, and G. A. Blake, Proc. Natl. Acad. Sci. USA **113**, 6857 (2016).

[4] P. Salen, M. Basini, S. Bonetti, J. Hebling, M. Krasilnikov, A. Y. Nikitin, G. Shamuilov, Z. Tibai, V. Zhaunerchyk, and V. Goryashko, Phys. Rep. **836**, 1 (2019).

[5] J. Waters, L. Froidevaux, R. Harwood, R. Jarnot, H. Pickett, W. Read, P. Siegel, R. Cofield, M. Filipiak, D. Flower, J. Holden, G. Lau, N. Livesey, G. Manney, H. Pumphrey, M. Santee, D. Wu, D. Cuddy, R. Lay, M. Loo, V. Perun, M. Schwartz, P. Stek, R. Thurstans, M. Boyles, K. Chandra, M. Chavez, G.-S. Chen, B. Chudasama, R. Dodge, R. Fuller, M. Girard, J. Jiang, Y. Jiang, B. Knosp, R. LaBelle, J. Lam, K. Lee, D. Miller, J. Oswald, N. Patel, D. Pukala, O. Quintero, D. Scaff, W. V. Snyder, M. Tope, P. Wagner, and M. Walch, IEEE T. Geosci. Remote **44**, 1075 (2006).

[6] Y. Yang, M. Mandehgar, and D. Grischkowsky, Opt. Express **22**, 4388 (2014).

[7] S.-C. Shi, S. Paine, Q.-J. Yao, Z.-H. Lin, X.-X. Li, W.-Y. Duan, H. Matsuo, Q. Zhang, J. Yang, M. C. B. Ashley, Z. Shang, and Z.-W. Hu, Nat. Astron. **1**, 1 (2017).

[8] T. M. Dame, D. Hartmann, and P. Thaddeus, Astrophys. J. **547**, 792 (2001).

[9] R. C. Kennicutt and N. J. Evans, Annu. Rev. Astron. Astrophys. **50**, 531 (2012).

[10] A. D. Bolatto, M. Wolfire, and A. K. Leroy, Annu. Rev. Astron. Astrophys. **51**, 207 (2013).

[11] V. C. Nibali and M. Havenith, J. Am. Chem. Soc. **136**, 12800 (2014).

[12] B. Ferguson and X.-C. Zhang, Nat. Mater. **1**, 26 (2002).

[13] M. Tonouchi, Nat. Photonics **1**, 97 (2007).

[14] T. Kampfrath, K. Tanaka, and K. Nelson, Nat. Photonics **7**, 680 (2013).

[15] S. S. Dhillon, M. S. Vitiello, E. H. Linfield, A. G. Davies, M. Hoffmann, J. H. Booske, C. Paoloni, M. Gensch, P. Weightman, G. P. Williams *et al.*, J. Phys. D: Appl. Phys. **50**, 043001 (2017).

[16] H. Li, Z. Li, W. Wan, K. Zhou, X. Liao, S. Yang, C. Wang, J. C. Cao, and H. Zeng, ACS Photonics **7**, 49 (2020).

[17] L. A. Sterczewski, J. Westberg, Y. Yang, D. Burghoff, J. Reno, Q. Hu, and G. Wysocki, ACS Photonics **7**, 1082 (2020).

[18] H. Elgabarty, T. Kampfrath, D. J. Bonthuis, V. Balos, N. K. Kaliannan, P. Loche, R. R. Netz, M. Wolf, T. D. Kühne, and M. Sajadi, Sci. Adv. **6**, eaay7074 (2020).

[19] K. J. Tielrooij, N. Garcia-Araez, M. Bonn, and H. J. Bakker, Science **328**, 1006 (2010).

[20] S. Funkner, G. Niehues, D. A. Schmidt, M. Heyden, G. Schwaab, K. M. Callahan, D. J. Tobias, and M. Havenith, J. Am. Chem. Soc. **134**, 1030 (2012).

[21] J. Savolainen, S. Ahmed, and P. Hamm, Proc. Natl. Acad. Sci. USA **110**, 20402 (2013).

[22] J. Lu, Y. Zhang, H. Y. Hwang, B. K. Ofori-Okai, S. Fleischer, and K. A. Nelson, Proc. Natl. Acad. Sci. USA **113**, 11800 (2016).

[23] M. B. Agranat, I. V. Il'na, and D. S. Sitnikov, High Temp. **55**, 922 (2017).

[24] P. Planken, Nature **456**, 454 (2008).

[25] S. J. Oh, J. Choi, I. Maeng, J. Y. Park, K. Lee, Y. M. Huh, J. S. Suh, S. Haam, and J. H. Son, Opt. Express **19**, 4009 (2011).

[26] F. Huth, A. Govyadinov, S. Amarie, W. Nuansing, F. Keilmann, and R. Hillenbrand, Nano Lett. **12**, 3973 (2012).

[27] C. Wu, A. B. Khanikaev, R. Adato, N. Arju, A. A. Yanik, H. Altug, and G. Shvets, Nat. Mater. **11**, 69 (2012).

[28] C. Shu, M. Autore, L. Jian, P. Li, and A. Y. Nikitin, ACS Photonics **4**, 3089 (2017).

[29] J. Zhang, X. Chen, S. Mills, T. Ciavatti, Z. Yao, R. Mescall, H. Hu, V. Semenenko, Z. Fei, H. Li, V. Perebeinos, H. Tao, Q. Dai, X. Du, and M. Liu, ACS Photonics **5**, 2645 (2018).

[30] Y. Liu, P. Ding, G. Lambert, A. Houard, V. Tikhonchuk, and A. Mysyrowicz, Phys. Rev. Lett. **115**, 133203 (2015).

[31] Y. Liu, P. Ding, N. Ibrakovic, S. Bengtsson, S. Chen, R. Danylo, E. R. Simpson, E. W. Larsen, X. Zhang, Z. Fan, A. Houard, J. Mauritsson, A. L'Huillier, C. L. Arnold, S. Zhuang, V. Tikhonchuk, and A. Mysyrowicz, Phys. Rev. Lett. **119**, 203205 (2017).

[32] J. Liu and X. C. Zhang, Phys. Rev. Lett. **103**, 235002 (2009).

[33] J. Liu, J. Dai, S. L. Chin, and X. C. Zhang, Nat. Photonics **4**, 627 (2010).

[34] R. Danylo, X. Zhang, Z. Fan, D. Zhou, Q. Lu, B. Zhou, Q. Liang, S. Zhuang, A. Houard, A. Mysyrowicz, E. Oliva, and Y. Liu, Phys. Rev. Lett. **123**, 243203 (2019).

[35] N. Karpowicz and X.-C. Zhang, Phys. Rev. Lett. **102**, 093001 (2009).

[36] Z. Zhang, Y. Chen, M. Chen, Z. Zhang, J. Yu, Z. Sheng, and J. Zhang, Phys. Rev. Lett. **117**, 243901 (2016).

[37] Z. Zheng, Y. Huang, Q. Guo, C. Meng, Z. Lu, X. Wang, J. Zhao, C. Meng, D. Zhang, J. Yuan, and Z. Zhao, Phys. Plasmas **24**, 103303 (2017).

[38] I. Thiele, B. Zhou, A. Nguyen, E. Smetanina, R. Nuter, K. J. Kaltenecker, P. G. de Alaiza Martínez, J. Déchard, L. Bergé, P. U. Jepsen, and S. Skupin, Optica **5**, 1617 (2018).

[39] Z. Mics, F. Kadlec, P. Kužel, P. Jungwirth, S. E. Bradforth, and V. A. Apkarian, J. Chem. Phys. **123**, 104310 (2005).

[40] R. Huber, F. Tauser, A. Brodschelm, M. Bichler, G. Abstreiter, and A. Leitenstorfer, Nature **414**, 286 (2001).

[41] Z. Mics, P. Kužel, P. Jungwirth, and S. E. Bradforth, Chem. Phys. Lett. **465**, 20 (2008).

[42] Y. Hu, X. H. Wang, L. T. Guo, and C. L. Zhang, Spectros. Spect. Anal. **26**, 1008 (2006).

[43] W. Aenchbacher, M. Naftaly, and R. Dudley, Appl. Opt. **49**, 2490 (2010).

[44] C. Townes and A. Schawlow, *Microwave Spectroscopy* (Dover, New York, 1975).

[45] H. Harde, S. Keiding, and D. Grischkowsky, Phys. Rev. Lett. **66**, 1834 (1991).

[46] B. Friedrich and D. R. Herschbach, Phys. Rev. Lett. **74**, 4623 (1995).

[47] I. V. Litvinyuk, K. F. Lee, P. W. Dooley, D. M. Rayner, D. M. Villeneuve, and P. B. Corkum, Phys. Rev. Lett. **90**, 233003 (2003).

[48] V. Ginzburg, *The Propagation of Electromagnetic Waves in Plasmas*, 2nd ed. (Pergamon Press, New York, 1970).

[49] J. Dai, J. Liu, and X. Zhang, IEEE J. Sel. Top. Quantum Electron. **17**, 183 (2011).

[50] J. Zhao, W. Chu, Z. Wang, Y. Peng, C. Gong, L. Lin, Y. Zhu, W. Liu, Y. Cheng, S. Zhuang, and Z. Xu, ACS Photonics **3**, 2338 (2016).

[51] Y. Itikawa, *Molecular Processes in Plasmas: Collisions of Charged Particles with Molecules* (Springer, Berlin, 2007).

[52] F. Buccheri and X.-C. Zhang, Optica **2**, 366 (2015).

[53] M. G. Kong, G. G. Kroesen, G. Morfill, T. Nosenko, T. Shimizu, van J Jan Dijk, and J. Zimmermann, New J. Phys. **11**, 115012 (2009).

[54] R. Pompl, F. Jamitzky, T. Shimizu, B. Steffes, W. Bunk, H.-U. Schmidt, M. Georgi, K. Ramrath, W. Stolz, R. W. Stark, T. Urayama, S. Fujii, and G. E. Morfill, New J. Phys. **11**, 115023 (2009).

[55] J. Liu and X.-C. Zhang, Front. Optoelectron. **7**, 156 (2014).

[56] P. Chevalier, A. Amirzhan, F. Wang, M. Piccardo, S. G. Johnson, F. Capasso, and H. O. Everitt, Science **366**, 856 (2019).

[57] M. F. Ciappina, J. A. Pérez-Hernández, A. S. Landsman, W. A. Okell, S. Zherebtsov, B. Förg, J. Schötz, L. Seiffert, T. Fennel, T. Shaaran, T. Zimmermann, A. Chacón, R. Guichard, A. Zaïr, J. W. G. Tisch, J. P. Marangos, T. Witting, A. Braun, S. A. Maier, L. Roso, M. Krüger, P. Hommelhoff, M. F. Kling, F. Krausz, and M. Lewenstein, Rep. Prog. Phys. **80**, 054401 (2017).

[58] J. Dai, X. Xie, and X.-C. Zhang, Phys. Rev. Lett. **97**, 103903 (2006).

[59] Z. Lü, D. Zhang, C. Meng, L. Sun, Z. Zhou, Z. Zhao, and J. Yuan, Appl. Phys. Lett. **101**, 081119 (2012).

[60] L. Keldysh, Sov. Phys. JETP **20**, 1307 (1965).

[61] M. Ammosov, N. Delone, and V. Krainov, Sov. Phys. JETP **64**, 1191 (1986).

[62] A. Becker, N. Aközbek, K. Vijayalakshmi, E. Oral, C. Bowden, and S. Chin, Appl. Phys. B **73**, 287 (2001).

[63] A. Couairon and A. Mysyrowicz, Phys. Rep. **441**, 47 (2007).

[64] J. H. Van Vleck and V. F. Weisskopf, Rev. Mod. Phys. **17**, 227 (1945).

[65] W. A. Stygar, G. A. Gerdin, and D. L. Fehl, Phys. Rev. E **66**, 046417 (2002).

[66] T. Kampfrath, D. O. Gericke, L. Perfetti, P. Tegeder, M. Wolf, and C. Frischkorn, Phys. Rev. E **76**, 066401 (2007).

[67] Y. Itikawa, J. Phys. Chem. Ref. Data **44**, 013105 (2015).

[68] A. E. Belikov, M. L. Strekalov, and A. V. Storozhev, Chem. Phys. Lett. **304**, 253 (1999).

[69] R. H. Dicke, Phys. Rev. **93**, 99 (1954).

[70] H. Sakai, C. P. Safvan, J. J. Larsen, K. M. Hilligso, K. Hald, and H. Stapelfeldt, J. Chem. Phys. **110**, 10235 (1999).

[71] J. Ortigoso, M. Rodríguez, M. Gupta, and B. Friedrich, J. Chem. Phys. **110**, 3870 (1999).

[72] S. De, I. Znakovskaya, D. Ray, F. Anis, N. G. Johnson, I. A. Bocharova, M. Magrakvelidze, B. D. Esry, C. L. Cocke, I. V. Litvinyuk, and M. F. Kling, Phys. Rev. Lett. **103**, 153002 (2009).